minerals

MDPI

Article

# New Approach for Direct Determination of Manganese Valence State in Ferromanganese Nodules by X-ray Fluorescence Spectrometry

**Victor M. Chubarov**

Vinogradov Institute of Geochemistry, Siberian Branch of the Russian Academy of Sciences, Favorsky St. 1A, 664033 Irkutsk, Russia; chubarov@igc.irk.ru

**Abstract:** A new X-ray fluorescence technique is proposed as an alternative to the labor-consuming volumetric method for the estimation of manganese valence state in ferromanganese nodules. The approach is based on the measurement of the relative intensities of some X-ray fluorescence spectrum characteristic spectral lines and satellites ($MnK\beta_5$ and $MnK\beta'$) preconditioned by electron transfer from the valence shell. Calibration curves were created using manganese oxide samples (MnO, $Mn_2O_3$, $MnO_2$) and 12 certified reference materials of ferromanganese nodules, cobalt-bearing ferromanganese crusts, and manganese ores with certified (or determined by approved methods) total and tetravalent manganese content. The presence of high iron content was taken into account. A set of oceanic ferromanganese nodules samples collected in the Magellan Seamounts (Pacific Ocean) were analyzed. Differences between the results of the X-ray fluorescence method and volumetric techniques for tetravalent manganese content were 4.9 rel.%, which is comparable with the accuracy of the volumetric technique (3.6 rel.%).

**Keywords:** wavelength-dispersive X-ray fluorescence; manganese valence state; ferromanganese nodules

check for updates

**Citation:** Chubarov, V.M. New Approach for Direct Determination of Manganese Valence State in Ferromanganese Nodules by X-ray Fluorescence Spectrometry. *Minerals* **2023**, *13*, 1329. https://doi.org/10.3390/min13101329

Academic Editors: Kiho Yang, Yongmoon Lee and Jaewoo Jung

Received: 8 September 2023
Revised: 5 October 2023
Accepted: 11 October 2023
Published: 14 October 2023



## 1. Introduction

In geological studies, the determination of the valence state of transition elements is the basis for assessing the redox conditions of rock formation [1] and, from a practical point of view, it is important for assessing the prospects for mining ores. Of all transition metals, there is only a routine method for determining the valence state of iron in geological objects. In mineral objects, iron has two main valence states, except metallic iron. Having information about at least one of them (divalent iron $Fe^{II}$ or trivalent iron $Fe^{III}$) and about total iron ($Fe^{total}$) content, it is possible to characterize iron valence state, for example as a ratio of ferrous (or ferric) and total iron. The determination of ferrous iron is widespread for the analysis of rocks using volumetric or spectrophotometric techniques [2–5].

In contrast to iron determination, the estimation of manganese valence state can be difficult. Manganese has three valence states in mineral objects (divalent manganese $Mn^{II}$, trivalent manganese $Mn^{III}$, and tetravalent manganese $Mn^{IV}$), and for the full characterization of the valence state besides total manganese ($Mn^{total}$) content, data on two of them are required. Determination of $Mn^{total}$ is a routine procedure. However, techniques for the diversification of manganese by valence states are rarely used [5–8]. These techniques are not as common as ones for ferrous iron and are used only in the analysis of manganese ores, since the rocks contain relatively low manganese. One of the types of specific manganese ores are ferromanganese nodules and crusts, which are a promising source of valuable metals (in addition to Mn and Fe, also Co, Ni, Cu, Zn, Pb, and rare earth and precious metals), despite the relatively difficult mining conditions [9,10]. When studying nodules and crusts, the valence state of ore elements is important for fundamental and application research and for assessing the ability of nodules to absorb valuable trace elements [11].

Despite the dominance of oxidized $Mn^{IV}$ (as asbolane, vernadite, todorokite, birnessite, buserite) and $Fe^{3+}$ (as oxides and hydroxides: goethite, limonite, ferroxigite, ferrihydrite, etc.), nodules can also contain other valence states of iron ($Fe^{II}$ as ilmenite or impurities in amphibole or pyroxene) and manganese ($Mn^{II}$ as impurities in todorokite and buserite and sometimes $Mn^{III}$ as impurities in birnessite) [12–14].

The X-ray fluorescence (XRF) method is widely used for the analysis of geological objects, including ferromanganese nodules and crusts [15–17]. Currently, the XRF method allows us not only to determine the total content of an element, but also to evaluate the forms of transition elements, including iron and manganese, based on the dependence of spectral lines intensities on the valence state of an element [18–20]. Parameters such as energy, intensity, and shape of lines preconditioned by the transitions of electrons from valence levels are the most affected by chemical bonding. There are $K\beta_5$ line and the most intense satellite $K\beta'$ for iron and manganese [21–32].

Despite our rather successful experience in the development of methods for the XRF determination of $Fe^{II}$ in different types of igneous rocks [32], this approach seems to be not applicable to ferromanganese nodules. There is no information on the content of ferrous iron (FeO) in certified reference materials (CRMs) of ferromanganese nodules. Besides, routine volumetric determination of ferrous iron in samples of ferromanganese nodules (as well as of ferromanganese ores) is impossible due to interference caused by high manganese content. Thus, the valence state of iron in ferromanganese nodules can only be assessed qualitatively as "close to $Fe^{III}$" [31]. However, in the case of manganese, the XRF method looks more promising, despite the relatively small (compared to rocks) number of CRMs of ferromanganese nodules [33]. The content of $MnO_2$ was certified (according to the certificate, by single visual titrimetry) in some CRMs of the SDO series [34]; moreover, the determination of $MnO_2$ in ferromanganese nodules can easily be carried out by reverse titration. In this work, the possibility to use the relative intensities of the $MnK\beta_5$ line and $MnK\beta'$ satellite of the XRF spectrum to determine manganese valence state in oceanic ferromanganese nodules is considered.

## 2. Materials and Methods

### *2.1. Equipment*

The investigation was carried out using the equipment of the Center for Isotopic and Geochemical Research (Vinogradov Institute of Geochemistry, Siberian Branch of the Russian Academy of Sciences, Irkutsk, Russian Federation) [35]. XRF spectra were studied using a S4 Pioneer wavelength-dispersive spectrometer (Bruker AXS, Karlsruhe, Germany) equipped with a Soller optical system, scintillation counter, and an X-ray tube with an Rh anode. All measurements were performed in vacuum mode using a lithium fluoride (LiF (220), 2d = 2.848 Å) crystal combined with a 0.23° collimator. A voltage of 50 kV and an X-ray tube current of 40 mA ensured a sufficient intensity of radiation. For spectra measurements, the step size was 0.024°, and the measurement time for each point was 4 s.

### *2.2. Samples*

To obtain the calibration, a set of CRMs was used. CRMs of ferromanganese nodules and cobalt-bearing ferromanganese crusts provided by the N. Fedorovsky All-Russian Scientific Research Institute of Mineral Raw Materials (CRM 408-10: GMK-1 and GMK-2, CRM 409-10: KMK-1 and KMK-2); the Research Institute of Applied Physics of Irkutsk State University together with the P.P. Shirshov Institute of Oceanology of the Russian Academy of Sciences OOPE601 (SDO-4), OOPE602 (SDO-5), OOPE603 (SDO-6) and OOPE604 (SDO-7) [34], sample certified during GeoPT proficiency testing program (FeMn-1 (GeoPT 23a)) [36]; and the Central Laboratory of Mongolia as a part of interlaboratory testing for certification (MnN) [37]; as well as three pure-grade manganese oxides (MnO, $Mn_2O_3$, $MnO_2$). Despite the large number of certified elements, only certificates for four CRMs of the SDO series [34] as well as a certificate for CRM MnN contained semi-quantitative data on the mineral composition (Table 1). For CRM 408-10 (GMK-1 and GMK-2), vernadite, todorokite

and birnessite were noted as the main Mn-containing minerals; aluminosilicates, plagioclase, and quartz were noted as the rock-forming minerals. For CRM 409-10 (KMK-1, and KMK-2), vernadite and apatite were noted as the main minerals; silicates, zeolite, quartz, and calcite were noted as the rock-forming minerals. For CRM FeMn-1, no data on mineral composition were found.

**Table 1.** Mineral composition of certified reference materials of ferromanganese nodules, %.

| Mineral | SDO-4 | SDO-5 | SDO-6 | SDO-7 | MnN |
|---|---|---|---|---|---|
| Asbolane | 35–40 | 15–20 | 8–12 | 6–10 | - |
| Vernadite | 4–6 | 3–5 | 5–7 | 20–25 | 80–85 |
| Todorokite | 3–5 | 15–20 | 10–15 | - | |
| Ferroxigite | 2–4 | 2–4 | 4–7 | 3–6 | - |
| Buzerite | - | 2–6 | 5–8 | - | - |
| Birnessite | - | 1–3 | 3–5 | - | - |
| Iron minerals [a] | 4–9 | 2–4 | 4–8 | 6–10 | 3–5 |
| Amorphous Fe and Mn phases | - | - | 5–8 | 2–4 | - |
| Silicate minerals [b] | 17–35 | 33–57 | 19–36 | 30–53 | 10–15 |
| Other minerals [c] | 8–13 | 6–11 | 3–6 | 7–13 | - |

[a] iron minerals are magnetite, ilmenite, and hematite; [b] silicate minerals are montmorillonite, hydrous micas, chlorite, pyroxene, amphibole, plagioclase, and feldspar; [c] other minerals are quartz, halite, and volcanic glass.

Certificates of only four of the listed ten CRMs contain data allowing us to estimate manganese valence state ($MnO_2$ iscertified in CRMs of SDO series); therefore, the other 8 samples were analyzed by volumetry (the technique will be described below). The calibration set was expanded using CRMs of manganese ores 5404-90 and 5407-90 with certified content of $MnO_2$ that contained predominantly $Mn^{II}$- and $Mn^{IV}$-containing minerals, including pyrolusite and psylomelane, as well as oxide and silicate manganese minerals (jacobsite, rhodonite, rhodochrosite, coronadite). CRMs of manganese ores were provided by Tsentrgeolanalit LLP (Karaganda, Kazakhstan). Other available CRMs of manganese ores contained a lot of $Mn^{III}$ as hausmanite, manganite, and braunite, and were not included in the calibration set.

For validation, a set of 15 samples of oceanic Co-bearing ferromanganese crusts collected on the Govorov and Kotzebue Guyots (Magellan Seamounts, Pacific Ocean) [38,39] were used.

Since the material of nodules and crusts is highly hygroscopic, all studied samples were dried at 120 °C for 48 h to constant weight to obtain air-dry samples. The content of hygroscopic moisture in the studied samples reached 15 wt.%. After drying, samples were pressed on a boric acid substrate and kept in a desiccator.

### *2.3. X-ray Fluorescence Kβ Spectra of Manganese*

According to its mineral composition, tetravalent manganese $Mn^{IV}$, as a compound of asbolane, vernadite, and todorokite, is the main compound of ferromanganese nodules. Figure 1 shows an XRF spectrum of a $Mn^{IV}$ oxide ($MnO_2$) sample in the energy range 6.42–6.57 keV. The most intense peak corresponds to the doublet $MnK\beta_{1,3}$ line (theoretical energy is 6490 eV here and below, according to the NIST database [40]) preconditioned by transitions $K\text{-}M_{2,3}$. This line has visual asymmetry in a low energy area that is related to the presence of relatively intense $MnK\beta'$ satellite interpreted as transitions $K\text{-}M_{2,3}$ (main $MnK\beta_{1,3}$ line) with a simultaneous ejection of an electron from level $M_{4,5}$. The relatively intense peak in the energy range 6.52–6.54 keV is the $MnK\beta_5$ line (theoretical value is 6535 eV) preconditioned by transitions $K\text{-}M_{4,5}$. According to [21], there are some satellites near the $MnK\beta_5$ line: $MnK\beta''$ (~6520 eV) and $MnK\beta'''$ (~6550 eV). Therefore, in fact, the peak in 6.52–6.54 keV energy range is a superposition of several lines. However, some of these lines do not appear for some compounds, and the resolution of the spectrometer is insufficient to split these peaks visually. Hence, for further study, the peak in the energy

range 6.52–6.54 keV was considered as the MnK$\beta_5$ line. To find a position for intensity measurement, a decomposition procedure was performed for the $MnO_2$ sample using the pseudo-Voigt function as a fitting function [41]:

$$F(E) = A\bullet(C_g\bullet G(E) + (1 - C_g)\bullet L(E)), \quad (1)$$

where $G(E) = \exp(-((E - Ep)/\sigma_g)^2)$ is Gaussian; $L(E) = 1/(1 + (((E - Ep)/\sigma_L)^2))$ is Lorentzian; A is the amplitude of the distribution centered at energy $E_p$; $\sigma_g$ and $\sigma_L$ are parameters defining the widths of the Gaussian and Lorentzian functions; $C_g$ determines the portion of Gaussian and Lorentzian and varies in the interval (0-1).

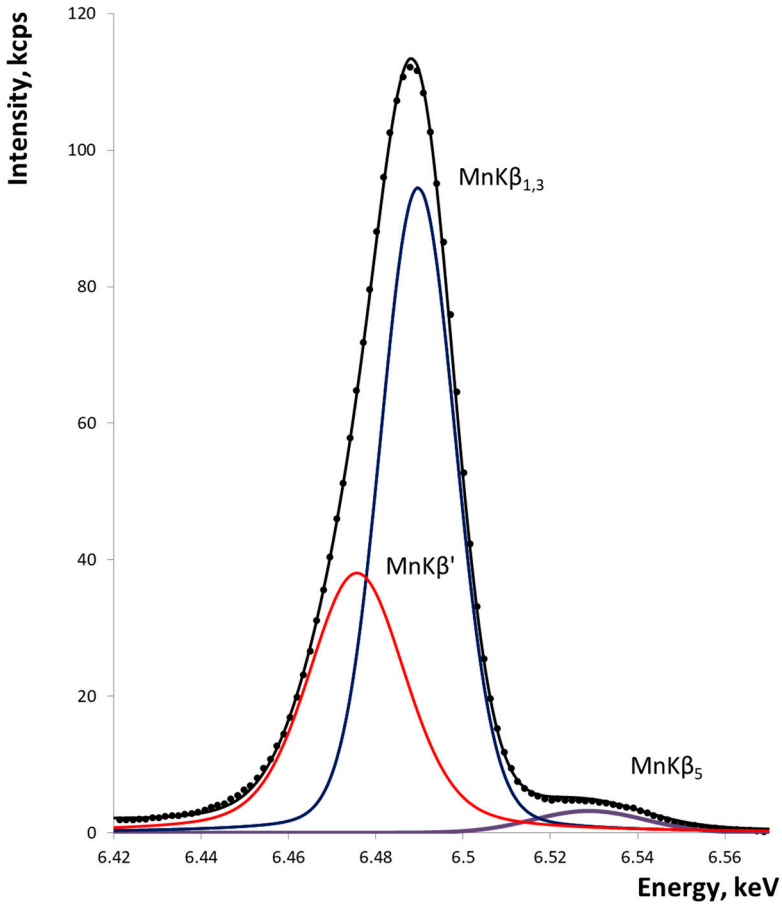


**Figure 1.** X-ray fluorescence spectrum in the field of MnK$\beta_{1,3}$ line for manganese (IV) oxide sample ($MnO_2$). Dots are measured spectrum; lines are results of decomposition using the pseudo-Voigt function.

According to decomposition, energy positions for analytical lines measurement were found as 6529 eV (MnK$\beta_5$) and 6469 eV (MnK$\beta'$). Because the intensity of any line of the manganese XRF spectrum depends on the gross manganese content, the ratios of selected lines to the intensity of line MnK$\beta_{1,3}$ were used as analytical parameters. To provide count rate statistic error at a level less than 1 rel.%, the exposition of measurement was defined as 10 s for the MnK$\beta_{1,3}$ line, 50 s for the MnK$\beta'$ line, and 100 s for the MnK$\beta_5$ line. Background intensity was measured in the 6590 eV energy position, where intense analytical lines of elements contained in ferromanganese nodules and crusts are absent.

Figure 2 shows the dependence and good convergence of the ratios of the MnK$\beta_5$/MnK$\beta_{1,3}$ and MnK$\beta'$/MnK$\beta_{1,3}$ line intensities on the manganese valence state ($N^{Mn}$) for manganese oxides. A polynomial equation was used for approximation.

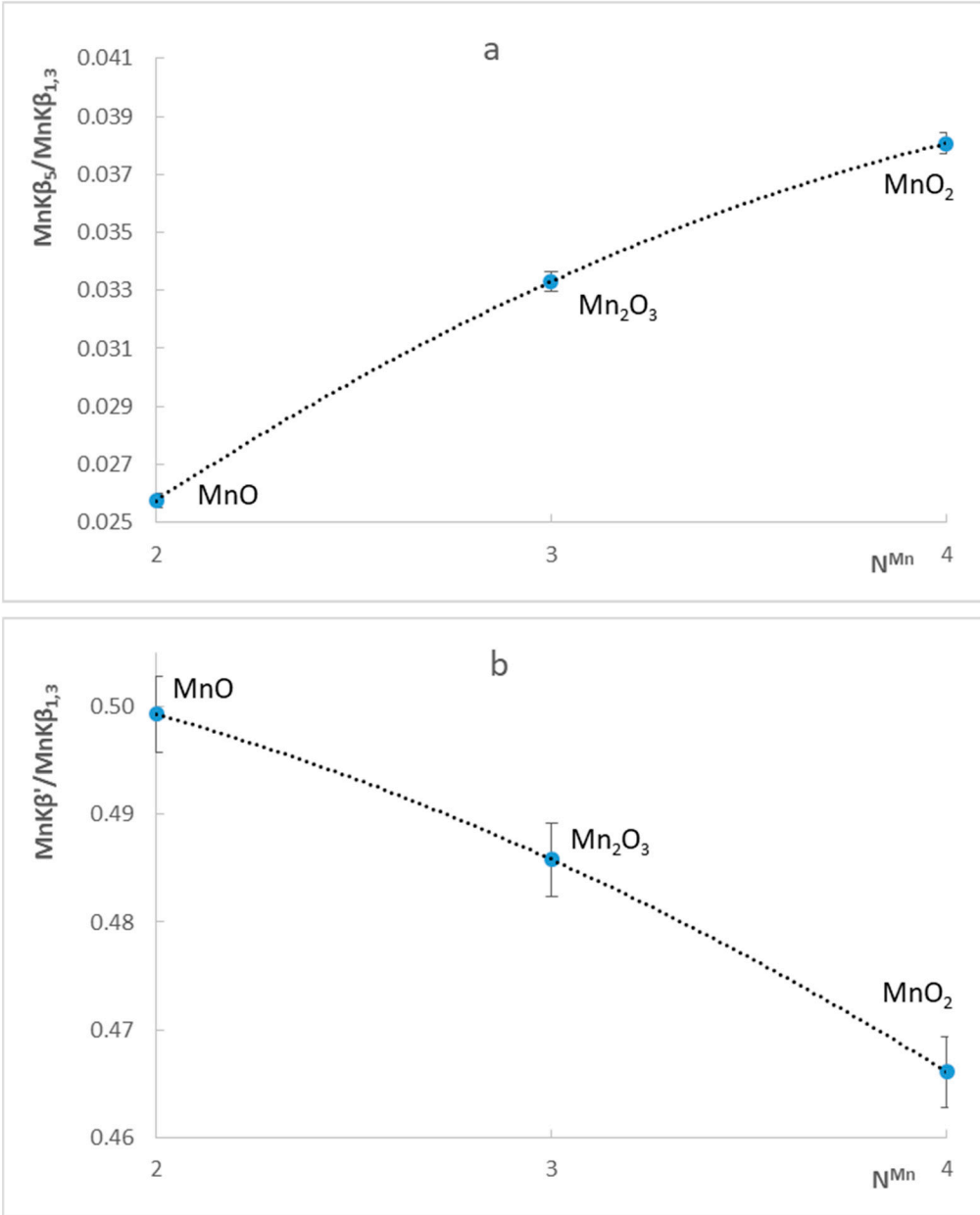


**Figure 2.** Dependence of ratios of line intensities of MnK$\beta_5$/MnK$\beta_{1,3}$ (**a**) and MnK$\beta'$/MnK$\beta_{1,3}$ (**b**) on the average manganese valence state ($N^{Mn}$) for three manganese oxide samples (MnO, $Mn_2O_3$, and $MnO_2$).

Unlike oxide, silicate, and carbonate ores, ferromanganese nodules have a specific phase and elemental composition; in particular, they contain high amounts of iron (in some cases exceeding the manganese content), which can significantly affect manganese line intensity due to possible spectral overlap with FeK$\alpha_{1,2}$ line. Figure 3 shows the XRF spectrum of the CRM of ferromanganese nodule SDO-4 with a total iron content of 12.05 wt.% and a total manganese content of 23.17 wt.%.

The spectral overlap between the FeK$\alpha_{1,2}$ line (theoretical energies are 6.391 keV and 6.404 keV) and manganese spectrum lines under consideration seems insignificant. But in cases where iron content is comparable to or exceeding manganese content (for example, in the CRM of ferromanganese nodule SDO-7, total iron and total manganese content is quite the same: 15.49 wt.% and 15.38 wt.%, respectively), the high intensity of FeK$\alpha_{1,2}$ lines can distort the measured intensities of selected manganese spectrum analytical lines. Moreover, the FeK$\beta$ line (7058 eV) excites the secondary fluorescence of manganese (energy

of manganese K edge is 6538 eV). There is a reason why, unlike silicate and carbonate manganese ores [30], the investigation of manganese valence state in ferromanganese nodules requires taking into account iron presence. The exposition of measurement of FeK$\alpha_{1,2}$ line was 10 s.

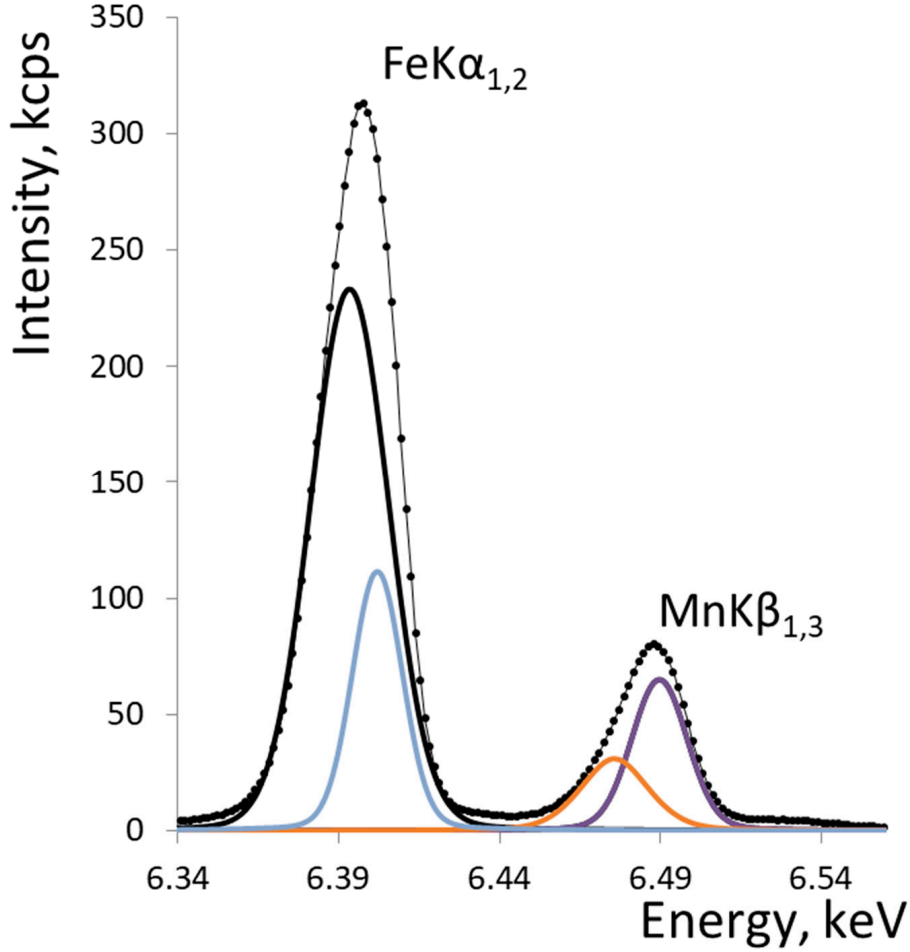


**Figure 3.** X-fluorescence spectrum in the field of MnK$\beta_{1,3}$ and FeK$\alpha_{1,2}$ lines of the CRM of ferromanganese nodule SDO-4. Dots are measured spectrum; lines are results of decomposition using the pseudo-Voigt function.

### *2.4. Manganese Valence State*

Because quantitative data on different valence state of manganese content in nodules are difficult to obtain, the only source for manganese valence state estimation is mineral composition, usually obtained by X-ray powder diffractometry. However, it is hard to find quantitative data on the mineral composition of nodules: the results of X-ray powder diffractometry analysis are often only qualitative, in particular due to the impossibility to identify amorphous iron and manganese minerals. Even CRMs often contain only semi-quantitative data (Table 1).

Taking into account the simultaneous presence of three main manganese valence states ($Mn^{II}$, $Mn^{III}$, and $Mn^{IV}$), the average manganese valence state of manganese can be calculated as:

$$N^{Mn} = \frac{2 \bullet C(Mn^{II}) + 3 \bullet C(Mn^{III}) + 4 \bullet C(Mn^{IV})}{C(Mn^{II}) + C(Mn^{III}) + C(Mn^{IV})}, \quad (2)$$

where $C(Mn^{II})$, $C(Mn^{III})$, and $C(Mn^{IV})$—content of divalent, trivalent, and tetravalent manganese, accordingly; 2, 3, and 4—manganese valence states.

According to data in the literature, nodules contain mainly $Mn^{IV}$-containing minerals with low quantities of $Mn^{II}$-containing minerals, usually in a mixture with $Mn^{IV}$ [12–14]; therefore, $N^{Mn}$ can be calculated only from the content of $Mn^{IV}$ and $Mn^{II}$ (as the difference between the content of $Mn^{total}$ and $Mn^{IV}$), accepting that content of $Mn^{III}$ is negligible.

Nonetheless, some minerals contain $Mn^{III}$ combined with $Mn^{II}$ and $Mn^{IV}$. For example, CRMs SDO-5 and SDO-6 contained up to 8% of buserite and up to 5% of birnessite (which together can contain up to 12% of $Mn^{III}$). This fact may have affected the accuracy of $N^{Mn}$ value calculation in Equation (2) if only $Mn^{II}$ and $Mn^{IV}$ content were used. For these two CRMs, $N^{Mn}$ values were calculated using Equation (2), assuming that both CRMs samples contained the maximal possible (taking into account phase composition, $Mn^{total}$, and $Mn^{IV}$ content) or no content of $Mn^{III}$. Due to the fact that the CRM SDO-5 has certified $MnO_2$ (31.01 ± 0.4 wt.%) and $MnO^{total}$ (25.16 ± 0.28 wt.%) content, recalculating to $Mn^{total}$ and $Mn^{IV}$ (due to the relatively wide confidence interval for $MnO_2$) leads to the conclusion that its content of $Mn^{IV}$ exceeds its content of $Mn^{total}$ (which is obviously impossible). Therefore, for the calculation, the highest and the lowest values in the confidence interval for $Mn^{total}$ and $Mn^{IV}$ content, respectively, were used. The calculated $N^{Mn}$ values were 3.95 and 3.90 (relative deviation is 1.3%) for CRM SDO-5 and 3.98 and 3.97 (relative deviation is 0.4%) for CRM SDO-6. These discrepancies will be discussed further.

To use all listed CRMs of ferromanganese nodules and crusts as a calibration set (and to analyze real samples of Co-bearing ferromanganese crusts), a certified volumetric technique was applied for the determination of $MnO_2$ content. The technique used is based on the reduction of $MnO_2$ by ammonium iron (II) sulfate $Fe(NH_4)_2(SO_4)_2$ and further titrating by potassium dichromate $K_2Cr_2O_7$ with sodium diphenylamine-4-sulfonate as the redox indicator.

To validate the volumetric technique, four CRMs of the SDO series (SDO-4, SDO-5, SDO-6, and SDO-7) with certified $MnO_2$ content were analyzed (Table 2). Repeatability was estimated by two independent measurements of CRMs SDO-4 and SDO-5; the deviations between results were 0.06 and 0.13 wt.%, respectively (less than 0.5 rel.%).

**Table 2.** Results of $MnO_2$ determination by volumetric technique ($MnO_2{}^{vt}$) in comparison with certified values ($MnO_2{}^{cert}$).

| CRM | $MnO_2{}^{cert} \pm \Delta$, wt.% | $MnO_2{}^{vt}$, wt.% | $N^{Mn,cert}$ | $N^{Mn,vt}$ |
|---|---|---|---|---|
| SDO-4 | 35.8 ± 0.4 | 34.9 | 3.95 | 3.90 |
| SDO-5 | 41.7 ± 0.5 | 40.1 | 3.94 | 3.87 |
| SDO-6 | 31.1 ± 0.4 | 29.6 | 4.00 | 3.92 |
| SDO-7 | 24.2 ± 0.4 | 23.5 | 3.99 | 3.93 |

A systematical underestimation from −0.7 to −1.6 wt.% (from 2.5 to 4.8 rel.%) of $MnO_2$ results obtained by the volumetric technique is observed; the standard deviation value for analyzed CRMs is 1.2 wt.% (3.6 rel.%), whereas the confidence interval of certified values is 0.4–0.5 wt.% (1.1–1.7 rel.%). Table 2 also contains the $N^{Mn}$ value calculated using Equation (2) from $MnO_2$ content obtained by volumetry or certified $MnO_2$ content, assuming that the content of trivalent manganese $C(Mn^{III})$ is insignificant. The relative standard deviation (RSD) for $N^{Mn}$ determination is 1.7%. In comparison with the case where $N^{Mn}$ values were calculated for CRMs SDO-5 and SDO-6, taking into account the possible presence of trivalent manganese $Mn^{III}$ (1.3 and 0.4 rel.%), errors in volumetric analysis were significantly higher (1.9 and 2.0 rel.%). Therefore, for further studies, it was accepted that ferromanganese nodules contain only divalent and tetravalent manganese ($Mn^{II}$ and $Mn^{IV}$), which corresponds to previous studies [12–14]. Table 3 shows the results of $MnO_2$ determination in 6 CRMs of ferromanganese nodules and Co-bearing ferromanganese crusts.

**Table 3.** $MnO_2$ content and average manganese valence state ($N^{Mn}$) determined by volumetric technique for CRMs of ferromanganese nodules.

| CRM | $MnO_2^{vt}$, wt.% | $N^{Mn,vt}$ |
|---|---|---|
| GMK-1 | 40.9 | 3.97 |
| GMK-2 | 43.6 | 3.98 |
| KMK-1 | 31.1 | 3.77 |
| KMK-2 | 20.3 | 3.79 |
| FeMn-1 | 47.5 | 3.65 |
| MnN | 41.9 | 3.77 |

## 3. Results and Discussion

### *3.1. Calibration*

To build calibration curves, 12 CRMs of ferromanganese nodules, Co-bearing ferromanganese crusts, and ores as well as three samples of manganese oxides were used. Ratios of $MnK\beta_5/MnK\beta_{1,3}$ and $MnK\beta'/MnK\beta_{1,3}$ line intensities were used as analytical parameters. The dependence of manganese valence state $N^{Mn}$ on analytical parameter $R^I$ was approximated by different variants of the equation:

$$N^{Mn} = a_0 + a_1 \bullet R^I + a_2 \bullet I(FeK\alpha_{1,2}) \quad (3)$$

where $N^{Mn}$—average manganese valence state, $R^I$—analytical parameter (ratio of analytical lines intensities), $I(FeK\alpha_{1,2})$—the intensity of the $FeK\alpha_{1,2}$ line included to take into account the presence of high iron content, $a_0$, $a_1$, $a_2$—coefficients of regression.

To discover the necessity of taking into account the presence of high iron content (as a possible spectral overlap of the $FeK\alpha_{1,2}$ line and the exciting of secondary fluorescence of manganese by the FeKβ line), Equation (3) with and without including the intensity of the $FeK\alpha_{1,2}$ line was also considered. The parameters of calibration curves (standard deviation (SD) and correlation coefficient ($r_{xy}$)) are shown in Table 4. Despite the fact that dependencies for three manganese oxides were approximated by a polynomial equation (Figure 2) for both the $MnK\beta_5/Mn\beta_{1,3}$ and $MnK\beta'/Mn\beta_{1,3}$ analytical parameters, for CRMs, polynomial equations did not lead to a significant decrease in SD value or significant increase in $r_{xy}$ value.

**Table 4.** Parameters of calibration curves.

| Equation Number | Analytical Parameter | Influence | $r_{xy}$ | SD |
|---|---|---|---|---|
| Equation (3.1) | $MnK\beta_5/Mn\beta_{1,3}$ | - | 0.63 | 0.32 |
| Equation (3.2) | | Fe | 0.94 | 0.13 |
| Equation (3.3) | $MnK\beta'/Mn\beta_{1,3}$ | - | 0.45 | 0.41 |
| Equation (3.4) | | Fe | 0.87 | 0.20 |
| Equation (3.5) | $MnK\beta_5/Mn\beta_{1,3}$, | - | 0.96 | 0.11 |
| Equation (3.6) | $MnK\beta'/Mn\beta_{1,3}$ | Fe | 0.97 | 0.09 |

As can be seen in Table 4, without taking into account the influence of iron presence, both $MnK\beta_5/Mn\beta_{1,3}$ and $MnK\beta'/Mn\beta_{1,3}$ provide the same poor accuracy (SD > 0.3, $r_{xy}$ < 0.70), whereas taking into account iron presence allows us to reduce SD value up to 2.5 times (Equations (3.2) and (3.4)). The minimal SD value (and sufficient $r_{xy}$ value more than 0.96) is observed when both analytical parameters are used (Equations (3.5) and (3.6)). However, in this case, the added intensity of the $FeK\alpha_{1,2}$ line as an additional member to Equation (3) does not allow us to significantly reduce SD value (Equation (3.6)). Probably, it is the close influence of iron presence for both the $MnK\beta_5$ and $MnK\beta'$ lines that compensates for this influence. Thus, four analytical parameters providing minimal SD values were used for further validation: ratios of $MnK\beta_5/Mn\beta_{1,3}$ and $MnK\beta'/Mn\beta_{1,3}$ line intensities with the intensity of the $FeK\alpha_{1,2}$ line as additional member (Equations (3.2)

and (3.4), respectively), and the combination of these ratios (Equations (3.5) and (3.6)). Coefficients of these four equations are shown in Supplementary Table S1. All selected equations have the same degrees of freedom (12). Figure 4 shows the correlations between $N^{Mn}$ values obtained from XRF analysis using different analytical parameters and ones calculated using Equation (2) for the calibration set.

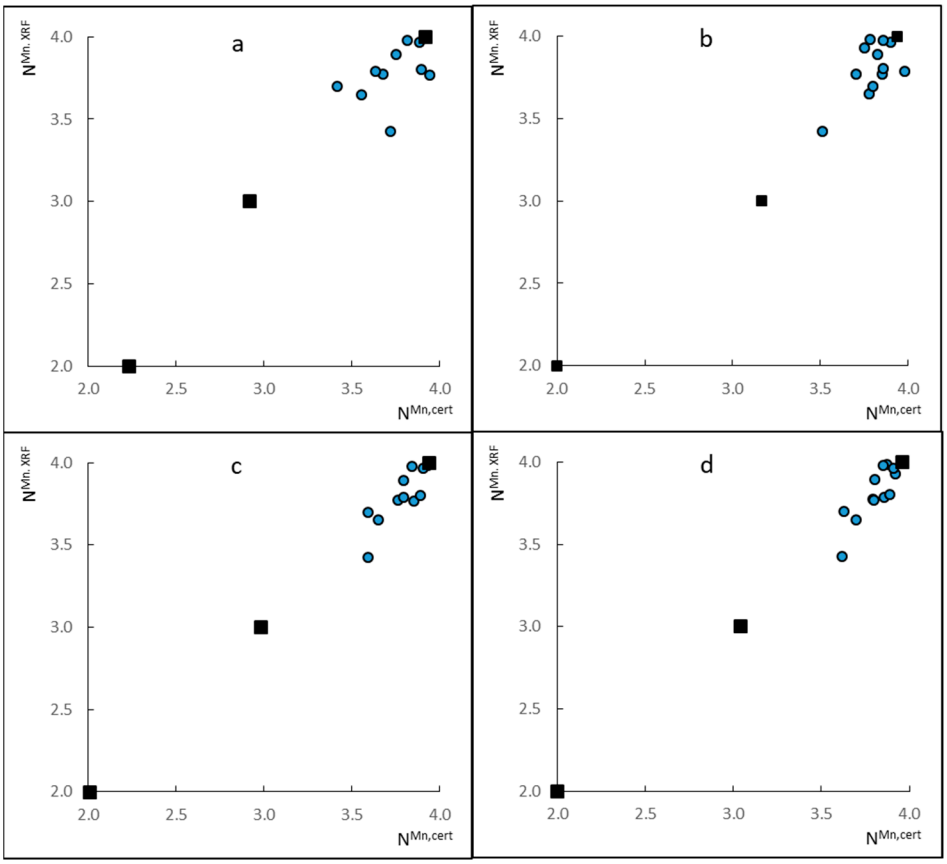


**Figure 4.** Correlations between $N^{Mn}$ values obtained from XRF analysis using different variants of Equation (3), see Table 4 and Table S2: Equation (3.2) (**a**), Equation (3.4) (**b**), Equation (3.5) (**c**), Equation (3.6) (**d**) and calculated using Equation (2) for the calibration set. Black squares are manganese oxides, blue dots are CRMs of ferromanganese nodules, Co-bearing ferromanganese crusts, and manganese ores.

### 3.2. Validation

For the validation of the proposed XRF technique, 15 samples of oceanic Co-bearing ferromanganese crusts collected on the Govorov and Kotzebue Guyots (Magellan Seamounts, Pacific Ocean) were studied. The content of $Mn^{total}$ was determined by the XRF method [17] and varied from 16.5 to 26.0 wt.%. Average manganese valence state was calculated from the volumetric results of $MnO_2$ determination and XRF results of $Mn^{total}$ determination using Equation (2), as well as directly determined by the proposed XRF technique using selected analytical parameters. Results are shown in Supplementary Table S2. $r_{xy}$ values between the obtained $N^{Mn}$ values were not more than 0.47, but this result is not informative for such a thin range of values (3.61–4.00). It can be concluded that most samples contained predominantly $Mn^{IV}$; however, in sample 3, $N^{Mn}$ was minimal in both XRF (3.61 using $MnK\beta_5/Mn\beta_{1,3}$ as an analytical parameter) and volumetric (3.59) results.

Table 5 shows a comparison of average valence state ($N^{Mn}$) values and recalculated $MnO_2$ content obtained by volumetric and proposed XRF techniques.

**Table 5.** The relative standard deviation for average manganese valence state determination (RSD ($N^{Mn}$)), relative standard deviation (SD ($MnO_2$)) and relative standard deviation (RSD ($MnO_2$)) for $MnO_2$ determination using different analytical parameters.

| Analytical Parameter | Influence | RSD ($N^{Mn}$), rel.% | SD ($MnO_2$), wt.% | RSD ($MnO_2$), rel.% |
|---|---|---|---|---|
| $MnK\beta_5/Mn\beta_{1,3}$ | Fe | 4.0 | 1.1 | 8.2 |
| $MnK\beta'/Mn\beta_{1,3}$ | Fe | 2.3 | 0.8 | 4.9 |
| $MnK\beta_5/Mn\beta_{1,3}$, | - | 2.5 | 0.8 | 5.1 |
| $MnK\beta'/Mn\beta_{1,3}$ | Fe | 3.1 | 1.0 | 6.2 |

As was concluded for manganese ores [41], the ratio of $MnK\beta'/Mn\beta_{1,3}$ line intensities is influenced by manganese speciation, but for samples with relatively close mineral composition, this parameter is optimal. The RSD value between $N^{Mn}$ results was 2.3%, which is comparable with the volumetry error (1.7 rel.%). When recalculating to $MnO_2$ content, SD was 0.8 wt.% (4.9 rel.%), which is comparable with a confidential interval of certified values (0.4–0.5 wt.%, or 1.3 rel.%).

## 4. Conclusions

The XRF method has been presented as a fast and cost-efficient method for estimating the valence state of manganese in ferromanganese nodules, where manganese occurs mainly as $Mn^{II}$ and $Mn^{IV}$. The accuracy of the proposed method was 4.9 rel.%, which is comparable with the accuracy of volumetric analysis (3.6 rel.%). The XRF method can be used to determine the valence state of manganese (simultaneously with the elemental XRF analysis of nodules) as an alternative to the labor- and time-consuming volumetric method.

**Supplementary Materials:** The following supporting information can be downloaded at: https://www.mdpi.com/article/10.3390/min13101329/s1, Table S1: Calibration curves; Table S2: Results of volumetric (vt) and XRF determination of average manganese valence state ($N^{Mn}$) and recalculation to $MnO_2$ content.

**Funding:** This research was funded by a grant from the Russian Science Foundation, grant number 23-23-00449, https://rscf.ru/project/23-23-00449/.

**Data Availability Statement:** Data are contained within the article or supplementary material.

**Acknowledgments:** This research was performed using the equipment of the Center for Isotopic and Geochemical Research (Vinogradov Institute of Geochemistry, Siberian Branch of the Russian Academy of Sciences, Irkutsk, Russian Federation). The author thanks Tatyana Ozhogina for the volumetric analysis, Roman Smely for the X-ray powder diffraction investigations, and Igor Peretjazhko for providing ferromanganese crust samples. Images for graphical abstract were taken from https://publicdomainvectors.org/, accessed on 1 July 2023.

**Conflicts of Interest:** The author declares no conflict of interest. The funders had no role in the design of the study; in the collection, analyses, or interpretation of data; in the writing of the manuscript; or in the decision to publish the results.

## References

1. Gaillard, F.; Pichavant, M.; Scaillet, B. Experimental determination of activities of FeO and $Fe_2O_3$ components in hydrous silicic melts under oxidizing conditions. *Geochim. Cosmochim. Acta* **2003**, *67*, 4389–4409. [CrossRef]
2. Andrade, S.; Hypolito, R.; Ulbrich, H.H.G.J.; Silva, M.L. Iron(II) oxide determination in rocks and minerals. *Chem. Geol.* **2002**, *182*, 85–89. [CrossRef]
3. Goldich, S.S. Determination of ferrous iron in silicate rocks. *Chem. Geol.* **1984**, *42*, 343–347. [CrossRef]
4. Whipple, E.R. A study of Wilson's determination of ferrous iron in silicates. *Chem. Geol.* **1974**, *14*, 223–238. [CrossRef]
5. Yokoyama, T.; Nakamura, E. Precise determination of ferrous iron in silicate rocks. *Geochim. Cosmochim. Acta* **2002**, *66*, 1085–1093. [CrossRef]
6. Zhou, H.; Mitamura, S. The Spectrophotometry Determination of Mn(III) in the Presence of Mn(IV). *Anal. Lett.* **1992**, *25*, 911–918. [CrossRef]

7. Zhu, Y.; Liang, X.; Zhao, H.; Yin, H.; Liu, M.; Liu, F.; Feng, X. Rapid determination of the Mn average oxidation state of Mn oxides with a novel two-step colorimetric method. *Anal. Methods* **2017**, *9*, 103–109. [CrossRef]
8. Song, Y.; Jiang, J.; Qin, W.; Zhu, J.; Gu, J.; Ma, J. Simultaneous photometric determination of oxidation kinetics and average manganese valence in manganese products in situ formed in the reactions of aqueous permanganate with model organic compounds and natural organic matters. *Sep. Purif. Technol.* **2021**, *256*, 117774. [CrossRef]
9. Halbach, P.E.; Jahn, A.; Cherkashov, G. Marine Co-Rich Ferromanganese Crust Deposits: Description and Formation, Occurrences and Distribution, Estimated World-wide Resources. In *Deep-Sea Mining: Resource Potential, Technical and Environmental Considerations*; Sharma, R., Ed.; Springer: Cham, Switzerland, 2017; pp. 65–141. [CrossRef]
10. Hein, J.R.; Koschinsky, A.; Kuhn, T. Deep-ocean polymetallic nodules as a resource for critical materials. *Nat. Rev. Earth Environ.* **2020**, *1*, 158–169. [CrossRef]
11. Brusnitsyn, A.I. Associations of Mn-bearing minerals as indicators of oxygen fugacity during the metamorphism of metalliferous deposits. *Geochem. Int.* **2007**, *45*, 345–363. [CrossRef]
12. Murray, J.W.; Balistrieri, L.S.; Paul, B. The oxidation state of manganese in marine sediments and ferromanganese nodules. *Geochim. Cosmochim. Acta* **1984**, *48*, 1237–1247. [CrossRef]
13. Pattan, J.N.; Mudholkar, A.V. The oxidation state of manganese in ferromanganese nodules and deep-sea sediments from the Central Indian Ocean. *Chem. Geol.* **1990**, *85*, 171–181. [CrossRef]
14. Kalhorn, S.; Emerson, S. The oxidation state of manganese in surface sediments of the deep sea. *Geochim. Cosmochim. Acta* **1984**, *48*, 897–902. [CrossRef]
15. Calvert, S.E.; Cousens, B.L.; Soon, M.Y.S. An X-ray fluorescence spectrometric method for the determination of major and minor elements in ferromanganese nodules. *Chem. Geol.* **1985**, *51*, 9–18. [CrossRef]
16. Cai, S.; Guo, Y.; Li, J. Comprehensive major, minor and trace element analysis of a submarine polymetallic nodule by wavelength-dispersive X-ray fluorescence spectrometry. *X-ray Spectrom.* **1992**, *21*, 17–20. [CrossRef]
17. Chubarov, V.; Amosova, A.; Finkelshtein, A. X-ray fluorescence determination of major elements in ferromanganese nodules. *X-ray Spectrom.* **2020**, *49*, 615–621. [CrossRef]
18. Kawai, J. *X-ray Spectroscopy for Chemical State Analysis*; Springer: Singapore, 2023. [CrossRef]
19. Mazalov, L.N.; Treiger, B.A. Chemical bonding effects in X-ray spectral analysis. *J. Struct. Chem.* **1983**, *24*, 276–305. [CrossRef]
20. Urch, D.S. Chemical Bonding Effects in X-ray Emission Spectra–A Molecular Orbital Model. *Adv. X-ray Anal.* **1970**, *14*, 250–267. [CrossRef]
21. Sakurai, K.; Eba, H. Chemical characterization using relative intensity of manganese $K\beta'$ and $K\beta_5$ X-ray fluorescence. *Nucl. Instrum. Methods B* **2003**, *199*, 391–395. [CrossRef]
22. Eba, H.; Sakurai, K. Site occupancy determination for manganese in some spinel-type oxides by $K\beta$ X-ray fluorescence spectra. *J. Solid State Chem.* **2005**, *178*, 370–375. [CrossRef]
23. Tsutsumi, K.; Nakamori, H.; Ichikawa, K. X-ray Mn $K\beta$ emission spectra of manganese oxides and manganates. *Phys. Rev. B* **1976**, *13*, 929. [CrossRef]
24. Tsutsumi, K. The X-ray Non-diagram Lines $K\beta'$ of Some Compounds of the Iron Group. *J. Phys. Soc. Jpn.* **1959**, *14*, 1696–1706. [CrossRef]
25. Asada, E.; Takiguchi, T.; Suzuki, Y. The effect of oxidation state on the intensities of $K\beta_5$ and $K\beta''$ of 3d-transition elements. *X-ray Spectrom.* **1975**, *4*, 186–189. [CrossRef]
26. Tamaki, Y. Chemical effect on intensity ratios of K-series X-rays in vanadium, chromium and manganese compounds. *X-ray Spectrom.* **1995**, *24*, 235–240. [CrossRef]
27. Fazinić, S.; Mandić, L.; Kavčič, M.; Božičevića, I. Parametrization of $K\beta''$ and $K\beta_{2,5}$ X-ray contributions in $K\beta$ spectra of 3d transition metal compounds. *J. Anal. At. Spectrom.* **2011**, *26*, 2467–2476. [CrossRef]
28. Limandri, S.; Ceppi, S.; Tirao, G.; Stutz, G.; Sánchez, C.G.; Riveros, J.A. High resolution study of $K\beta'$ and $K\beta_{1,3}$ X-ray emission lines from Mn-compounds. *Chem. Phys.* **2010**, *367*, 93–98. [CrossRef]
29. Volkov, A.I.; Ossipov, K.B.; Seregin, A.N.; Zhdanov, P.A.; Seregina, I.F.; Bolshov, M.A. Determination of degree of oxidation and forms of manganese compounds in the Ulu-Telyak oxidized ore. *Inorg. Mater.* **2015**, *51*, 1394–1403. [CrossRef]
30. Chubarov, V.; Suvorova, D.; Mukhetdinova, A.; Finkelshtein, A. X-ray fluorescence determination of the manganese valence state and speciation in manganese ores. *X-ray Spectrom.* **2015**, *44*, 436–441. [CrossRef]
31. Chubarov, V.M.; Finkelshtein, A.L.; Granina, L.Z. Determination of content and valence state of iron and Manganese in nodules using K-series emission lines of X-ray fluorescence spectrum. *Anal. Control* **2010**, *14*, 65–72. (In Russian)
32. Chubarov, V.M.; Finkelshtein, A.L. Determination of divalent iron content in igneous rocks of ultrabasic, basic and intermediate compositions by a wavelength-dispersive X-ray fluorescence spectrometric method. *Spectrochim. Acta B* **2015**, *107*, 110–114. [CrossRef]
33. Wang, Y.; Song, H.; Wang, X. Ocean manganese nodule and sediment reference materials. *Mar. Georesour. Geotechnol.* **2008**, *16*, 321–334. [CrossRef]
34. Berkovits, L.A.; Obolyaninova, V.G.; Parshin, A.P.; Romanovskaya, A.R. A system of sediment reference samples: OO. *Geostand. Newsl.* **1991**, *15*, 85–109. [CrossRef]

35. Skuzovatov, S.Y.; Belozerova, O.Y.; Vasil'eva, I.E.; Zarubina, O.V.; Kaneva, E.V.; Sokolnikova, Y.V.; Chubarov, V.M.; Shabanova, E.V. Centre of Isotopic and Geochemical Research (IGC SB RAS): Current State of Micro- and Macroanalysis. *Geodyn. Tectonophys.* **2022**, *13*, 0585. [CrossRef]
36. Kriete, C. An Evaluation of the Inter-Method Discrepancies in Ferromanganese Nodule Proficiency Test GeoPT 23A. *Geostand. Geoanal. Res.* **2011**, *35*, 319–340. [CrossRef]
37. Batjargal, B.; Davaasuren, B.; Erdenetsetseg, D. Producing Certified Reference Materials at the Central Geological Laboratory of Mongolia. *Geostand. Geoanal. Res.* **2010**, *34*, 231–236. [CrossRef]
38. Novikov, G.V.; Sedysheva, T.E.; Lobkovsky, L.I.; Lobus, N.V.; Bogdanova, O.Y. Ore Content of Cobalt-Rich Ferromanganese Crusts of the Govorov Guyot of the Magellanic Mountains of the Pacific Ocean. *Dokl. Earth Sci.* **2021**, *499*, 675–682. [CrossRef]
39. Novikov, G.V.; Sedysheva, T.E.; Bogdanova, O.Y.; Lobus, N.V. Cobalt-rich ferromanganese crusts of the Kotzebue Guyot of the Magellan Seamounts of the pacific ocean: Conditions of occurrence, mineralogy, and geochemistry. *Oceanology* **2022**, *62*, 879–889. [CrossRef]
40. Deslattes, R.D.; Kessler, E.G., Jr.; Indelicato, P.; de Billy, L.; Lindroth, E.; Anton, J.; Coursey, J.S.; Schwab, D.J.; Chang, J.; Sukumar, R.; et al. *X-ray Transition Energies Database*; NIST Standard Reference Database 128; NIST: Gaithersburg, MD, USA, 2003. [CrossRef]
41. Remond, G.; Myklebust, R.; Fialin, M.; Nockolds, C.; Phillips, M.; Roques-Carmes, C. Decomposition of wavelength dispersive X-ray spectra. *J. Res. Natl. Inst. Stand. Technol.* **2002**, *107*, 509–529. [CrossRef] [PubMed]